nature COMMUNICATIONS

ARTICLE

Received 15 May 2013 | Accepted 22 Sep 2013 | Published 5 Nov 2013

DOI: 10.1038/ncomms3655

Huge critical current density and tailored superconducting anisotropy in $SmFeAsO_{0.8}F_{0.15}$ by low-density columnar-defect incorporation

L. Fang[1], Y. Jia[1], V. Mishra[1], C. Chaparro[1], V.K. Vlasko-Vlasov[1], A.E. Koshelev[1], U. Welp[1], G.W. Crabtree[1], S. Zhu[2], N.D. Zhigadlo[3], S. Katrych[3,4], J. Karpinski[3,4] & W.K. Kwok[1]

Iron-based superconductors could be useful for electricity distribution and superconducting magnet applications because of their relatively high critical current densities and upper critical fields. $SmFeAsO_{0.8}F_{0.15}$ is of particular interest as it has the highest transition temperature among these materials. Here we show that by introducing a low density of correlated nano-scale defects into this material by heavy-ion irradiation, we can increase its critical current density to up to 2×10^7 A cm^{-2} at 5 K—the highest ever reported for an iron-based superconductor—without reducing its critical temperature of 50 K. We also observe a notable reduction in the thermodynamic superconducting anisotropy, from 8 to 4 upon irradiation. We develop a model based on anisotropic electron scattering that predicts that the superconducting anisotropy can be tailored via correlated defects in semimetallic, fully gapped type II superconductors.

[1] Materials Science Division, Argonne National Laboratory, Argonne, Illinois 60439, USA. [2] Physics Division, Argonne National Laboratory, Argonne, Illinois 60439, USA. [3] Laboratory for Solid State Physics, ETH Zurich, Schafmattstrasse 16, CH-8093 Zurich, Switzerland. [4] Institute of Condensed Matter Physics EPFL, CH-1015 Lausanne, Switzerland. Correspondence and requests for materials should be addressed to L.F. (email: lfang@anl.gov) or to W.K.K. (email: wkwok@anl.gov).

The reasonably high values of the superconducting transition temperature T_c, very high upper critical magnetic fields and generally low anisotropy of the recently discovered iron-based superconductors[1–3] enable operation in economically interesting temperature-field ranges and, at the same time, minimize detrimental effects due to grain boundaries and thermal fluctuations[4,5]. However, the overriding application metric, the maximum loss-less electrical current density, is ultimately determined by the vortex pinning that can be engineered into the material. Significant advances towards high-performing superconducting materials based on the so-called 122-compounds, most notably $Ba(Fe_{1-x}Co_x)_2As_2$ and $Ba_{1-x}K_xFe_2As_2$ (refs 6–8), and 11-compounds[9] have been made. For instance, $Ba_{0.6}K_{0.4}Fe_2As_2$ has demonstrated a nearly field-independent critical current density of $J_c = 5\,MA\,cm^{-2}$ at 5 K and H ~ 7 T (ref. 10). These $J_c(T,H)$ values are comparable to state-of-the-art $YBa_2Cu_3O_{7-\delta}$ (YBCO)-coated conductors under similar conditions. However, the relatively low values of T_c, 23 and 38 K, respectively, pose serious limitations. FeAs-1111 compounds, such as $SmFeAsO_{1-x}F_x$, have T_c in excess of 50 K (ref. 11). In addition, high critical current densities approaching 1–2 MA cm^{-2} in as-grown $SmFeAsO_{1-x}F_x$ crystals and films at 5 K and self-field have been reported[12–14]. However, the layered structure of $SmFeAsO_{1-x}F_x$, shown in Fig. 1a, leads to a rather high anisotropy, $\gamma \sim 8$ (refs 15,16), exceeding that of YBCO, which causes the suppression of the irreversibility field and limitation of applications at high fields and high temperature. To mitigate these drawbacks, nano-scale columnar defects in optimal-doped $SmFeAsO_{0.8}F_{0.15}$ crystals were produced. Columnar defects have been proven very effective in vortex pinning in high-T_c cuprates[17] as they are capable of trapping vortices over extended sections of their length (see Fig. 1b). To date, the performance of $SmFeAsO_{0.8}F_{0.15}$ with columnar pinning landscape is unknown, and the ceiling of J_c of the iron-based superconductors remains an open question.

Here we incorporated a low density of columnar defects into pristine $SmFeAsO_{0.8}F_{0.15}$ crystals using high-energy, heavy-ion irradiation along the c-axis. The induced columnar defects produce record-high values of the critical current density without degradation of the transition temperature. The enhanced critical current to J_c (5 K, 0 T) ≈ 20 MA cm^{-2} corresponds to ~20% of the depairing current. Furthermore, we found a pronounced reduction in the superconducting anisotropy from 8 to 4 following the irradiation. Such a phenomenon can be qualitatively understood in the framework of anisotropic electron scattering by columnar defects.

Results

Columnar-defect incorporation. $SmFeAsO_{0.8}F_{0.15}$ single crystals with an approximate size of $100 \times 100 \times 6\,\mu m^3$ (shown in Fig. 1c) and submicrogram mass were grown at ETH Zurich in a high-pressure synthesis procedure using NaCl/KCl flux[18,19]. Two $SmFeAsO_{0.8}F_{0.15}$ crystals were irradiated at the ATLAS facility at Argonne National Laboratory with 1.4-GeV Pb –ions to doses of $N = 2 \times 10^{11}$ (sample no. 1) and 5×10^{11} ions cm^{-2} (sample no. 2), corresponding to nominal dose-matching fields of $B_\Phi = 4$ and 9.5 T along the crystal's c-axis; $B_\Phi = N\Phi_0$, where $\Phi_0 = 2.07 \times 10^{15}\,Tm^2$. Heavy-ion irradiation leaves amorphous tracks (columnar defects) where the ions have traversed through

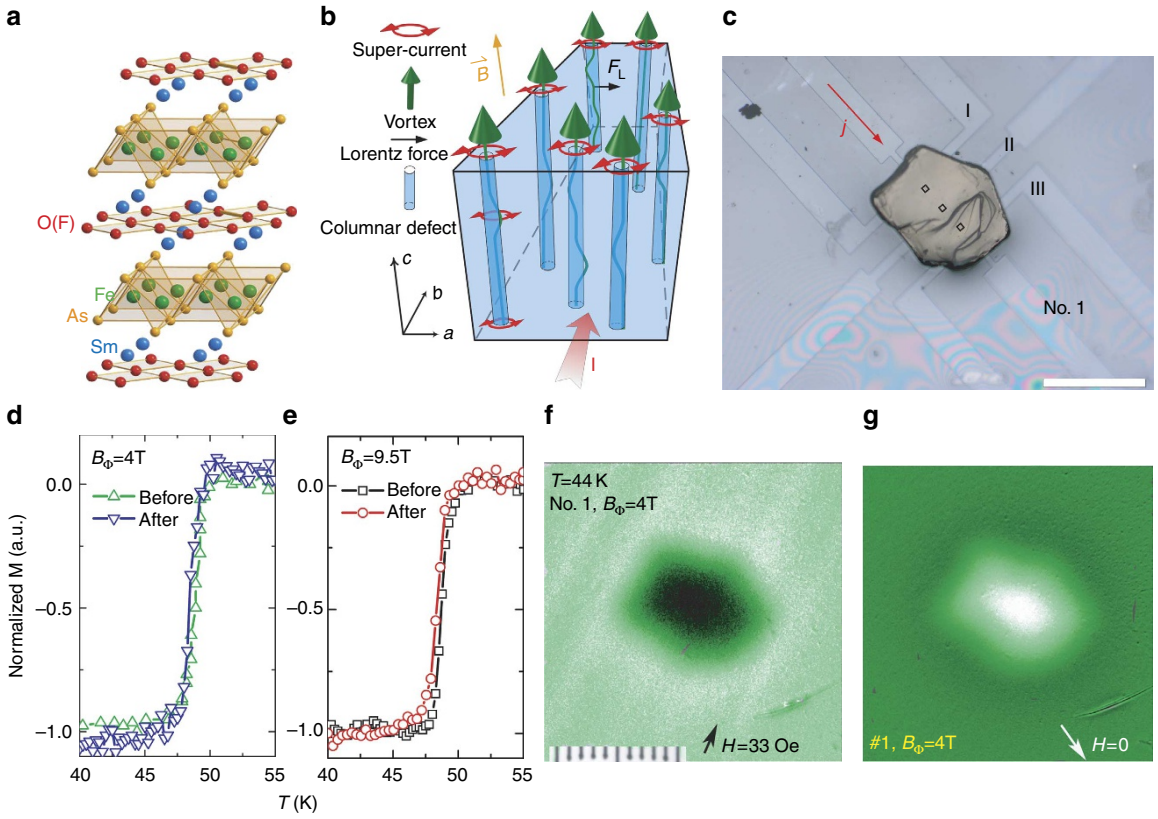

Figure 1 | Heavy-ion-irradiated $SmFeAsO_{0.8}F_{0.15}$ and magnetization characterizations. a and **b** are schematic pictures of the layered structure of $SmFeAsO_{1-x}F_x$ and of the correlated nano-scale defects produced by the high energy, heavy-ion irradiation. (**c**) Image of sample no. 1 placed on top of a micro-Hall array magnetometer. The black open squares represent the position of the individual Hall-probe sensing areas underneath the crystal. (**d**) and (**e**) Magnetization measurements of sample no. 1 and no. 2, pre- and post irradiation. T_c remains virtually unchanged following irradiation. (**f**) and (**g**) Magneto-optical imaging of magnetic flux in sample no. 1 in increasing and decreasing applied magnetic fields. The scale bars in (**c**) and (**f**) represent 100 μm.

the sample[20]. Compared with the structural density of 6×10^{14} unit cells cm^{-2} for $SmFeAsO_{0.8}F_{0.15}$, the concentration of tracks is rather dilute, ~2–5 tracks per 1,000 unit cells.

Transition temperatures. Figure 1d,e shows SQUID magnetic measurements in a field of 1 Oe (H//c) after zero-field cooling for the two $SmFeAsO_{0.8}F_{0.15}$ crystals before and after irradiation. We observe a temperature-independent magnetic moment at low temperatures and a sharp superconducting transition at $T_c = 50$ K with $\Delta T_c \sim 1.5$ K, underlining the high quality of the crystals. Our results show that the transition temperature and transition width do not change appreciably for irradiation doses up to 9.5 T. Similar robust transition temperatures against heavy-ion-induced defects were observed in $Ba_{0.6}K_{0.4}Fe_2As_2$ crystals with 1.4-GeV Pb-ion irradiation doses up to $B_\Phi = 21$ T (ref. 10). These results suggest that in both, the FeAs-1111 and the FeAs-122-compounds, columnar defects induce non-magnetic small-angle intra-band scattering, which does not contribute to pair-breaking for s$\pm$-gap symmetry.

Critical current densities. The small size of the crystals used in our study precludes the use of a commercial SQUID magnetometer to obtain J_c through magnetic hysteresis measurements at temperatures above 20 K. We therefore placed the crystal onto a highly sensitive micro-Hall-array magnetometer (see Fig. 1c). The crystal was carefully aligned with a high precision manipulator to ensure that the same position within 5 μm was maintained for measurements before and after irradiation, corresponding to an uncertainty of <10%. The black squares in Fig. 1c denote the three active areas of the Hall-array, with the middle sensor located at the centre of the crystal. A magneto-optical (MO) indicator film technique[21] was used to check for weak links such as grain boundaries in the samples. The images of field screening and trapped flux after switching off the external magnetic field are shown in Fig. 1f,g for sample no. 1. No weak-link areas for preferential entry/exit of vortices can be detected, confirming the single grain and homogeneous critical current density behaviour over the entire sample.

Figure 2a compares the magnetic hysteresis loops at the centre of sample no. 2 at $T = 10$ K before and after irradiation to a dose of $B_\Phi = 9.5$ T. A ten-fold enhancement can be observed for the irradiated sample. This large enhancement factor is observed over the entire temperature range from $T = 5$ to 40 K. For comparison between local and global magnetization measurements, we measured the magnetization hysteresis curve of sample no. 2 with a SQUID magnetometer at $T = 5$ K, where the signal was large enough to be detected from the small crystals. Using the Bean model[22] $J_c = 20\Delta M/a(1\text{-}a/3b)$, we obtained J_c values from the hysteresis loop width, ΔM. A calibration factor was obtained by comparing the J_c value determined by SQUID magnetometry at low temperature and the J_c values obtained from the micro-Hall-array magnetometer. This factor was used to convert the micro-Hall-array data to J_c values at high temperatures. The derived $J_c(H,T)$-values for the 9.5-T-irradiated sample no. 2 at various temperatures and fields are presented in Fig. 2b. At 5 K and self-field, the critical current density is remarkably high $J_c = 1.8 \sim 2 \times 10^7$ A cm^{-2}, whereas J_c at 44 K and 0 T is 2×10^5 A cm^{-2}. As for the 4 T-irradiated sample no. 1, the critical current derived using the same method yields $J_c = 9 \times 10^6$ A cm^{-2} at 5 and 0 T, ~4.5 times the J_c (5 K, 0 T) of the pristine sample. The depairing current of $SmFeAsO_{0.85}F_{0.15}$ can be estimated by $j_0 = \frac{\Phi_0}{3\sqrt{3}\mu_0\pi\lambda^2\xi^{ab}}$, where Φ_0 is the flux quantum,

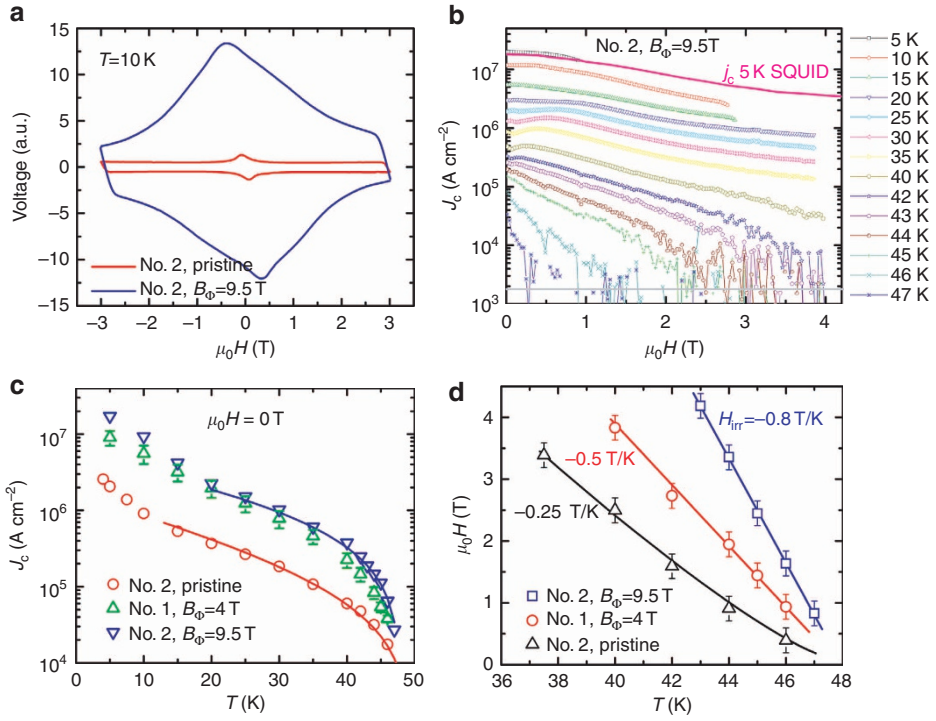

Figure 2 | Critical current density and irreversibility field of irradiated $SmFeAsO_{0.8}F_{0.15}$. (**a**) Micro-Hall-bar voltage signal from the middle sensor for sample no. 2 before and after irradiation to a dose-matching field of $B_\Phi = 9.5$ T. (**b**) Magnetic field dependence of J_c at various temperatures for sample no. 2. The magenta solid line is the J_c determined from SQUID measurements at $T = 5$ K using the Bean model calculation. The open symbols are J_c obtained from the micro-Hall-array magnetometer. (**c**) J_c as a function of temperature for the pre-irradiated sample no. 1, postirradiated sample no. 1 ($B_\Phi = 4$ T) and sample no. 2 ($B_\Phi = 9.5$ T). 10% J_c uncertainty of postirradiated sample no. 1 arises from the different determinations between measurements of Hall array and magneto-optical imaging. (**d**) The irreversibility line for the investigated three samples. $J_c = 2{,}000$ A cm^{-2} was used as a criterion to determine the irreversibility fields. Uncertainty comes from the noise in J_c measurement which is shown in **b**. The solid lines in **c** and **d** are guides to the eye.

and using values of the penetration depth $\lambda \sim 200$ nm and the coherence length $\xi^{ab}(0) \sim 1.5$ nm (refs 2,16,23). The calculated value of $j_0 \sim 1 \times 10^8$ A cm^{-2} indicates that we have achieved $\sim 20\%$ of the depairing current by simply incorporating a low density of columnar defects. To the best of our knowledge, such a high J_c value has not been reported on any of the iron-based superconductors. This is a remarkably high J_c for a single crystal, considering that even in state-of-the-art YBCO conductors, the self-field J_c has reached only 15–25% of the depairing current after a decade of pinning landscape engineering[24–26]. By increasing the density of defects and by combining different types of pinning centres into $SmFeAsO_{0.8}F_{0.15}$, further enhancement of J_c can be expected.

Figure 2c shows the temperature dependence of J_c before and after irradiation. The order-of-magnitude enhancement of J_c due to irradiation is apparent over the entire temperature range. The initial (almost) exponential decrease of J_c with temperature followed by a power-law variation has been observed for several 1111-materials[27]. It has been suggested that at low field (self-field) and low temperatures, strong single-vortex pinning is dominant[27], whereas at higher temperature, effects due to collective pinning and creep become important. Using a criterion of $J_c = 2 \times 10^3$ A cm^{-2}, we determined the irreversibility line H_{irr}. The slope of H_{irr} increases by a factor of 2–3 after irradiation, as shown in Fig. 2d. These results demonstrate that a low density of columnar defects can firmly pin the vortices and effectively extend the useful range in the H–T phase diagram into the vortex liquid region.

Thermodynamic superconducting anisotropy and model. Another remarkable aspect of columnar defects is the surprising reduction of the thermodynamic superconducting anisotropy. Here, we use a highly sensitive membrane-based steady-state *ac* micro-calorimeter to measure the specific heat of the sub-microgram crystals[28] and to determine the superconducting anisotropy. The specific heat anomaly near $T_c \sim 50$ K of sample no. 1 in zero field is delineated in Fig. 3a. Subtraction of the normal state background as described in detail in Welp *et al.*[16] yields the superconducting specific heat near the transition as shown in Fig. 3b for the pristine and $B_\Phi = 4$ T irradiated sample no. 1, respectively. The height of the cusp-like anomaly of sample no. 1 before irradiation (pristine) is ~ 24 mJ per mol K^2. After irradiation, the height of the C/T anomaly is slightly suppressed, which can be attributed to a fractional loss of the superconducting material due to the formation of amorphous damage tracks. The transition temperature as revealed by specific heat does not change appreciably with irradiation, in agreement with the magnetic characterization, shown in Fig. 1d,e.

The superconducting anisotropy can be directly obtained by comparing the resulting heat capacity anomaly at T_c when the magnetic field is applied along the c-axis and ab-plane of the crystal. As shown in Fig. 3c, the specific heat data for 0.5 T//c and 4.0 T//ab coincide, revealing a superconducting anisotropy of $\gamma \sim 8$ in the pristine $SmFeAsO_{0.8}F_{0.15}$ crystal. Similarly, in the irradiated samples with doses of $B_\Phi = 4$ T and $B_\Phi = 9.5$ T, the temperature-dependent C/T curves at 0.5 T//c overlap with those at 2.0 T//ab, corresponding to an anisotropy of $\gamma \sim 4$ (Fig. 3d,e). This result indicates that the incorporation of a low density of columnar defects reduces the superconducting anisotropy of $SmFeAsO_{0.85}F_{0.15}$ by one half without changing the transition temperature. This tailoring of the anisotropy reduces the Ginzburg number and thereby enhances the irreversibility line and vortex pinning in irradiated $SmFeAsO_{0.8}F_{0.15}$.

Our results can be qualitatively accounted for in a model based on anisotropic scattering by columnar defects. In the case of a dilute concentration of scattering centres, point defects mix all momentum states equally, whereas extended defects preserve the

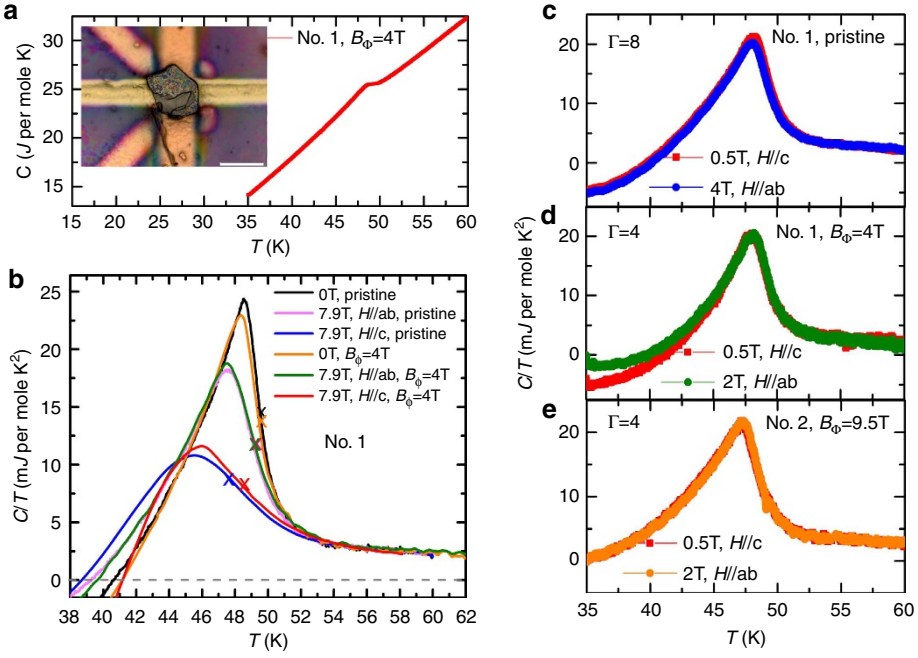

Figure 3 | Heat capacity and superconducting anisotropy of irradiated $SmFeAsO_{0.8}F_{0.15}$. (**a**) Temperature-dependent specific heat of sample no. 1 irradiated to a matching field of $B_\Phi = 4$ T. The anomaly due to the superconducting transition near 49 K is clearly seen. The inset shows sample no. 1 with a size $\sim 120 \times 90 \times 6\ \mu m^3$ placed on top of the ac micro-calorimeter. (**b**) The electronic heat capacity anomaly near T_c for pristine sample no. 1 (before irradiation) and after irradiation ($B_\Phi = 4$ T). The crosses mark the transition temperature as determined from the inflection point of $\partial C(T)/\partial T$. (**c**–**e**) Temperature-dependent specific heat at fixed fields for H||c and H||ab to determine the superconducting anisotropy γ. The ratio of the two orthogonal fields for which the C/T curves coincide is the anisotropy γ.

momentum along certain directions[29]. For columnar defects, the momentum along the column's axis is preserved, which is the c-axis in our case. Therefore, after irradiation the electron mean free path l along the c-axis remains the same, whereas l in the ab-plane decreases due to additional scattering from the columns. This can be qualitatively described as $1/l^{c} = 1/l_0^{c}$ and $1/l^{ab} = 1/l_0^{ab} + 1/l_{irr}$, where l_0^{c} and l^{c} represent the c-axis electron mean free path prior and post irradiation. Likewise, l_0^{ab} and l^{ab} denote the in-plane mean free paths. l_{irr} is the average distance travelled by an electron between two consecutive scattering events from two columns. The anisotropy parameter γ is defined as,

$$\gamma = \frac{dH_{C2}^{H\|ab}}{dT} \Big/ \frac{dH_{C2}^{H\|c}}{dT} \quad (1)$$

where the upper critical fields $H_{c2}^{H\|ab}$ and $H_{c2}^{H\|c}$ are determined in Ginzburg–Landau theory through the in-plane and out-of-plane coherence lengths ξ^{ab} and ξ^{c} (ref. 30), $H_{c2}^{H\|ab} = \Phi_0/2\pi\xi^{ab}\xi^{c}$ and $H_{c2}^{H\|c} = \Phi_0/2\pi(\xi^{ab})^2$. For the qualitative description given here, we consider identical electron bands or the dominance of one major band in a two-band superconductor, which reduces to the one-band scenario for the upper critical field[31,32]. The change in anisotropy induced by the anisotropic scattering due to columnar defects can be expressed in terms of the change of the coherence lengths for both the clean and dirty limits. As presented in more detail in the Supplementary Notes 1 and 2, the anisotropy parameter γ for a single-band superconductor in the clean limit can be expressed as

$$\frac{\gamma}{\gamma_0} = \frac{1}{1 + \frac{\xi_P^{ab}}{l_{irr}}} \text{ for } l_0^{ab} \ll \xi_0^{ab} \quad (2)$$

here γ_0 and l_0^{ab} denote the anisotropy and mean free path of the unirradiated sample, ξ_0^{ab} is the BCS (Bardeen-Cooper-Schrieffer) (or Pippard) coherence length, and $1/\xi_P^{ab} = 1/\xi_0^{ab} + 1/l_0^{ab}$ is the inverse of the pre-irradiation coherence length. Correspondingly, the anisotropy parameter γ for a single-band superconductor in the dirty limit reads

$$\frac{\gamma}{\gamma_0} = \sqrt{\frac{l^{ab}}{l^{c}}} = \frac{1}{\sqrt{1 + \frac{l_0^{ab}}{l_{irr}}}} \text{ for } l_0^{ab} \ll \xi_0^{ab} \quad (3)$$

Equations 2 and 3 reveal for both limiting cases that the additional electron scattering by columnar defects, represented by l_{irr}, leads to a reduction of the superconducting anisotropy. As shown in Supplementary Fig. S1, γ decreases rapidly with increasing defect at low concentrations and levels off at higher concentrations. These results are qualitatively consistent with our experimental observation that at higher defect concentration the anisotropy does not decrease any further within the uncertainties. A quantitative description of the data will require precise knowledge of the relation between l_{irr} and the number of columns and a microscopic modelling of the electron scattering induced by these defects, which are beyond the ambit of this paper. In any case, by incorporating columnar defects along the c-axis, the thermodynamic superconducting anisotropy can be reduced. The rate of reduction with increasing irradiation-induced columnar defects is determined by the number of pre-existing defects, carrier density and the scattering potential of the columnar defects. As the in-plane and out-of-plane upper critical fields are given by $H_{c2}^{H\|ab} = \Phi_0/2\pi\xi^{ab}\xi^{c}$ and $H_{c2}^{H\|c} = \Phi_0/2\pi(\xi^{ab})^2$, the reduction of ξ^{ab} brought by anisotropic electron scattering causes a larger enhancement of $H_{c2}^{H\|c}$ than of $H_{c2}^{H\|ab}$ as is directly shown in Fig. 3b for sample no. 1. The enhancement of dH_{c2}/dT is 2 for fields along the c-axis and 1.2 for fields applied in the plane. The crosses in Fig. 3b mark the superconducting transition temperatures that correspond approximately to the inflection points of C/T according to pervious analysis of the specific heat data of $SmFeAsO_{1-x}F_x$ (ref. 16).

Discussion

A reduction of the anisotropy after heavy-ion irradiation with virtually unchanged T_c was also observed in 122-compounds. For example, the anisotropy of $Ba_{0.6}K_{0.4}Fe_2As_2$ is reduced from 2.5 to 2.1 after 1.4 GeV Pb-ion irradiation to a dose of $B_\Phi = 21$ T (ref. 10); heavy-ion-irradiated $SrFe_2(As_{1-x}P_x)_2$ shows an anisotropy change from 1.6–1.5 to 1.2–1.3 (ref. 33). The comparatively small reduction of anisotropy in the FeAs-122 materials can be attributed to the initial low anisotropy and the discontinuous morphology of the damage tracks[10]. Similar phenomena could be expected in high-T_c cuprates, MgB_2 and other anisotropic superconductors. Very limited attention has been paid to the reduction of the superconducting anisotropy due to correlated defects in these materials. In the case of cuprates, any change of H_{c2} is convoluted with a reduction of T_c, whereas the high conductivity of MgB_2 and of most conventional superconductors has prevented the creation of columnar defects with heavy-ion irradiation[34]. For iron-based superconductors, their semimetal property and weak gap anisotropy[2] enable us to tune the anisotropy via heavy-ion irradiation. We expect other poor-metallic and fully gapped type II superconductors to follow our predictions and demonstrate tailored anisotropy as well. This general phenomenon is important for the application of new superconducting materials.

The low anisotropy, high critical current and high T_c indicate that optimal-doped $SmFeAsO_{1-x}F_x$ may be the best iron-based superconductor for application. Recent progress in $SmFeAsO_{1-x}F_x$ thin film synthesis has provided the premise for fabricating high-quality films using appropriate substrates[13,14]. Further improvement of the performance of these films can be expected when columnar-type defects are incorporated. Experiences accumulated over the past decades on creating self-assembled columnar defects in cuprates films[35] via chemical synthesis could help promote similar critical current enhancement in iron-based superconducting films. In this respect, $SmFeAsO_{1-x}F_x$-based superconducting products with performance comparable to the state-of-the-art of cuprates can be expected.

Methods

Specific heat measurement. We applied a membrane-based steady-state *ac* micro-calorimeter to measure the calorimetric effect of submicrogram single crystals. It utilizes a thermocouple composed of Au-1.7% Co and Cu films deposited onto a 150-nm-thick Si_3N_4 membrane as a thermometer. $SmFeAsO_{0.8}F_{0.15}$ crystals with a size $\sim 100 \times 100 \times 6\,\mu m^3$ were mounted on the thermocouple using Apiezon N grease. An ac-heater current at low frequency (< 200 Hz) is adjusted such as to induce oscillations of the sample temperature of 50–200 mK.

Critical current measurement. The Hall sensor is based on a two-dimensional electron gas GaAs/AlGaAs heterostructure. The Hall-bar array was fabricated by photolithography and chemical etching. The active area is $5 \times 5\,\mu m^2$ and the sensitivity is 0.27 Ω per Gauss. The low temperature magnetization was measured by a SQUID (Quantum Design) magnetometer with a resolution down to 2×10^{-8} emu. For both Hall sensor and SQUID measurements, the magnetic field was applied in a step mode and the magnetic responses were measured after a 10-s stabilization time.

J_c determination using the MO images. A high spatial-resolution (down to 1 μm) MO imaging technique was used to map the magnetic induction component, B_z, normal to the crystals' ab-plane. It is based on the Faraday rotation of polarized

light in a garnet indicator film placed on top of the sample. The field profile of the trapped flux, $\boldsymbol{B}_z(x)$ allows us to estimate the critical current density either by numerically integrating Biot–Savart's law for the supercurrent flow pattern inside the sample or by using an approximate expression for the normal component of the magnetic induction in elongated rectangular thin samples.

$$\boldsymbol{B}_z = \frac{\mu_0}{4\pi}\int \frac{d\mathbf{i}\times\mathbf{r}}{r^2} \approx \frac{\mu_0 J_C t}{4\pi}\, ln\, \frac{\left[z_0^2+\left(x-\frac{a}{2}\right)^2\right]\left[z_0^2+\left(x+\frac{a}{2}\right)^2\right]}{\left[z_0^2+x^2\right]^2} \qquad (4)$$

here, $t = 6\,\mu m$ is the thickness of the sample, a is width and z_0 the gap between the MO indicator film and the sample surface. z_0 is obtained from the ratio of the maximum $\boldsymbol{B}_z$ at the centre and minimum negative $\boldsymbol{B}_z$ near the sample edge $k = \boldsymbol{B}_z^{max}/|\boldsymbol{B}_z^{min}|$, which for a known sample geometry is a unique function of z_0 (ref. 36). In our case, $k \sim 10$ gives the indicator position $z_0 \sim 10\,\mu m$ and the critical current density $\sim 10^5\,A\,cm^{-2}$, in good agreement with estimates of J_c from the M(H) loops.

References

1. Kamihara, Y., Watanabe, T., Hirano, M. & Hosono, H. Iron-based layered superconductor La[$O_{1-x}F_x$]FeAs ($x = 0.05$–0.12) with $T_c = 26$ K. *J. Am. Chem. Soc.* **130,** 3296–3297 (2008).
2. Johnston, D. C. The puzzle of high temperature superconductivity in layered iron pnictides and chalcogenides. *Adv. Phys.* **59,** 803–1061 (2010).
3. Tanabe, K. & Hosono, H. Frontiers of research on iron-based superconductors toward their application. *Jpn J. Appl. Phys.* **51,** 010005 (2012).
4. Gurevich, A. To use or not to use cool superconductors? *Nat. Mater.* **10,** 255–259 (2011).
5. Katase, T. *et al.* Advantageous grain boundaries in ion pnictide superconductors. *Nat. Commun.* **2,** 409 (2011).
6. Weiss, J.D. *et al.* High intergrain critical current density in fine-grain $(Ba_{0.6}K_{0.4})Fe_2As_2$ wires and bulks. *Nat. Mater.* **11**(8): 682–685 (2012).
7. Ma, Y. Progress in wire fabrication of iron-based superconductors. *Supercond. Sci. Technol.* **25,** 113001 (2012).
8. Lee, S. *et al.* Artificially engineered superlattices of pnictide superconductors. *Nat. Mater.* **12,** 392–396 (2013).
9. Si, W. *et al.* High-current superconductivity $FeSe_{0.5}Te_{0.5}$-coated conductors at 30 tesla. *Nat. Commun.* **4,** 1347 (2013).
10. Fang, L. *et al.* High, magnetic field independent critical currents in $(Ba,K)Fe_2As_2$ crystals. *Appl. Phys. Lett.* **101,** 012601 (2012).
11. Ren, Z. *et al.* Superconductivity at 55 K in iron-based F-doped layered quaternary compound Sm($O_{1-x}F_x$)FeAs. *Chin. Phy. Lett.* **25,** 2215–2216 (2008).
12. Moll, P. J. W. *et al.* High magnetic-field scales and critical currents in SmFeAs(O,F) crystals. *Nat. Mater.* **9,** 628–633 (2010).
13. Takeda, S. T. *et al.* Growth of superconducting SmFeAs(O,F) epitaxial films by F diffusion. *Supercond. Sci. Technol.* **25,** 035007 (2012).
14. Iida, K. *et al.* Oxypnictide SmFeAs(O,F) superconductor: a candidate for high-field magnet applications. *Sci. Rep.* **3,** 2139 (2013).
15. Weyeneth, S. *et al.* Anisotropy of superconducting single crystal $SmFeAsO_{0.8}F_{0.2}$ studied by torque magnetometry. *J. Supercond. Novel Magn.* **22,** 325–329 (2009).
16. Welp, U. *et al.* Anisotropic phase diagram and superconducting fluctuations of single-crystalline $SmFeAsO_{0.85}F_{0.15}$. *Phys. Rev. B* **83,** 100513(R) (2011).
17. Civale, L. Vortex pinning and creep in high-temperature superconductors with columnar defects. *Supercond. Sci. Technol.* **10,** A11–A28 (1997).
18. Zhigadlo, N.D. *et al.* Single crystals of superconducting $SmFeAsO_{1-x}F_y$ grown at high pressure. *J. Phys. Condens. Matter* **20,** 342202 (2008).
19. Karpinski, J *et al.* Single crystals of $LnFeAsO_{1-x}F_x$ (Ln = La, Pr, Nd, Sm, Gd) and $Ba_{1-x}Rb_xFe_2As_2$: growth, structure and superconducting properties. *Physica C* **469,** 370–380 (2009).
20. Moore, J. D. *et al.* The effect of columnar defects on the pinning properties of $NdFeAsO_{0.8}$ conglomerate particles. *Supercond. Sci. Technol.* **22,** 125023 (2009).
21. Welp, U., Vlasko-Vlasov, V. K., Liu, X., Furdyna, J. K. & Wojtowicz, T. Magnetic domain structure and magnetic anisotropy in $Ga_{1-x}Mn_xAs$. *Phys. Rev. Lett.* **90,** 167206 (2003).
22. Bean, C. P. Magnetization of high-field superconductors. *Rev. Modern Phys.* **36,** 31–39 (1964).
23. Drew, A. J. *et al.* Coexistence of magnetic fluctuations and superconductivity in the pnictide high temperature superconductor $SmFeAsO_{1-x}F_x$ measured by muon spin rotation. *Phys. Rev. Lett.* **101,** 097010 (2008).
24. Sarrao, J. & Kwok, W. K. *Basic Research Needs for Superconductivity*. US DOE, Washington, DC, USA (2006) http://www.science.energy.gov/~/media/bes/pdf/reports/files/sc_rpt.pdf.
25. Miura, M. *et al.* Mixed pinning landscape in nanoparticle-introduced $YGdBa_2Cu_3O_y$ films grown by metal organic deposition. *Phys. Rev. B* **83,** 184519 (2011).
26. Chen, Z. *et al.* A high critical current density MOCVD coated conductor with strong vortex pinning centers suitable for very high field use. *Supercond. Sci. Technol.* **22,** 055013 (2009).
27. van der Beek, C. J. *et al.* Flux pinning in $PrFeAsO_{0.9}$ and $NdFeAsO_{0.9}F_{0.1}$ superconducting crystals. *Phys. Rev. B* **81,** 174517 (2010).
28. Tagliati, S., Krasnov, V. M. & Rydh, A. Differential membrane-based nanocalorimeter for high-resolution measurements of low-temperature specific heat. *Rev. Sci. Instrum.* **83,** 055107 (2012).
29. Durst, A. C. & Lee, P. A. Microwave conductivity due to scattering from extended linear defects in d-wave superconductors. *Phys. Rev. B* **65,** 094501 (2002).
30. Tinkham, M. *Introduction to Superconductivity* (McGraw-Hill, 1996).
31. Gurevich, A. Enhancement of the upper critical field by nonmagnetic impurities in dirty two-gap superconductors. *Phys. Rev. B* **67,** 184515 (2003).
32. Golubov, A. A. & Koshelev, A. E. Upper critical field in dirty two-band superconductors: Breakdown of the anisotropic Ginzburg-Landau theory. *Phys. Rev. B* **68,** 104503 (2003).
33. Yeninas, S. *et al.* Upper critical field of isoelectron substituted $SrFe_2(As_{1-x}P_x)_2$. *Phys. Rev. B* **87,** 094503 (2013).
34. Chikumoto, N., Yamamoto, A., Konczykowski, M. & Murakami, M. Magnetization behavior of MgB_2 and the effect of high energy heavy-ion irradiation. *Physica C* **378-381,** 466–469 (2002).
35. Macmanus-Driscoll, J. L. *et al.* Strongly enhanced critical current densities in superconducting coated conductors of $YBa_2Cu_3O_{7-x}$ + $BaZrO_3$. *Nat. Mater.* **3,** 439–443 (2004).
36. Welp, U., Xiao, Z. L., Novosad, V. & Vlasko-Vlasov, V. K. Commensurability and strong vortex pinning in nanopatterned Nb films. *Phys. Rev. B* **71,** 014505 (2005).

Acknowledgements

Critical current measurements and theory were supported by the Center for Emergent Superconductivity, an Energy Frontier Research Center funded by the US Department of Energy, Office of Science, Office of Basic Energy Sciences (L.F., Y.J., V.M., A.E.K., W.K.K., G.W.C.), specific heat and magneto-optical measurements were supported by the Department of Energy, Office of Basic Energy Sciences, under Contract No. DE-AC02-06CH11357 (C.C., V.K.V.-V., U.W.). J.K. and S.K. acknowledge support of the EC Research Council project SuperIron. N.D.Z. acknowledges the support of the Swiss National Science Foundation and the National Center of Competence in Research MaNEP (Materials with Novel Electronic Properties).

Author contributions

N. D. Z., S. K., J.K. grew the crystals and performed x-ray refinement. L.F., Y.J., C.C., V.K.V.-V., S.Z., U.W., W.K.K. conducted the experiments. V.M. and L.F. modelled the theory. L.F., Y.J., U.W., W.K.K., A.E.K. and G.W.C. discussed the data. L.F., U.W. and W.K.K. analysed the data and prepared the manuscript.

Additional information

Supplementary Information accompanies this paper at http://www.nature.com/naturecommunications.

Competing financial interests: The authors declare no competing financial interests.

Reprints and permission information is available online at http://www.nature.com/reprintsandpermissions.

How to cite this article: Fang, L. *et al.* Huge critical current density and tailored superconducting anisotropy in $SmFeAsO_{0.8}F_{0.15}$ by low-density columnar-defect incorporation. *Nat. Commun.* 4:2655 doi: 10.1038/ncomms3655 (2013).